International Journal of Environmental Science and Technology (2020) 17:4265–4280
https://doi.org/10.1007/s13762-020-02753-6

ORIGINAL PAPER

Development of eco-friendly, self-cleaning, antibacterial membrane for the elimination of chromium (VI) from tannery wastewater

Z. Arif[1] · N. K. Sethy[1] · P. K. Mishra[1] · B. Verma[1]

Received: 21 January 2020 / Revised: 19 March 2020 / Accepted: 17 April 2020 / Published online: 29 April 2020

Abstract

Hydrophobic polyvinylidene fluoride membrane was reformed to the hydrophilic membrane by incorporating synthesized titanium dioxide nanoparticles using *Cajanus cajan* seed extract. Spectroscopic and microscopic techniques characterized the composite membrane. The X-ray diffraction confirms the anatase phase of titanium dioxide nanoparticles of crystalline size 15.89 nm. The effect of titanium dioxide concentration on the thermodynamical and rheological properties on the polyvinylidene fluoride casting solution was investigated by the triangle phase diagram and viscosity measurement. It was concluded that titanium dioxide introduction caused thermodynamic enhancement, but the impact of rheological hinderance was higher at high concentrations. The polyvinylidene fluoride/titanium dioxide membranes were used as a bi-functional membrane to evaluate the rejection of chromium (VI) from wastewater; then, they were applied as sunlight-active catalyst membrane to reduce the concentrated chromium (VI) to chromium (III) by reduction. It was concluded that at 0.02 wt% of titanium dioxide, the maximum rejection of 85.59% and *a*% reduction of 92% was achieved with enhanced flux.

Keywords Nanoparticles · Phase diagram · Membrane · Separation technique · Catalyst

Introduction

The growing concentration of hazardous chemicals discharged from industries force the government organization to put a restriction on them to limit their discharge. Over a decade, the chromium (VI) is considered as significant contaminants causing health risks among living beings (Loryuenyong et al. 2014). The different source for the existence of hexavalent chromium includes leather tanning, chromate production, paint making and electroplating having discharge concentration ranging from 2000 to 5000 mg/mL but recommended permissible limit is only 2 mg/mL (Belay 2010). One solution to eradicate carcinogenic chromium (VI) is to convert into a non-toxic Cr (III) state, which is also an essential trace metal as human nutrition. The conventional chemical technique needs expensive reducing agents like ferrous sulfate, sodium hydrogen sulfite, sodium pyrosulfite and hydrazine hydrate. Also, they are harmful to living beings, human skin and release unwanted chemicals (Dhala et al. 2013). Table 1 lists the pros and cons of different conventional, existing and emergent techniques for removal of a pollutant from wastewater (Abdullah et al. 2019; Crini and Lichtfouse 2019; Burakov et al. 2018).

Recently, membrane separation has been widely used to treat wastewater. The low permeate flux with high operating pressure increases the cost in the case of reverse osmosis (RO) and nanofiltration (NF). Hence, ultrafiltration processes are preferred more as they work at low transmembrane pressures with lower operating costs. However, the use of membrane can only remove Cr (VI) ions from permeate and is acceptable according to environmental standards, but Cr (VI) concentration goes on increasing overtime at the retentate side and needs to be treated further before discharging to the environment. This problem intensifies more when the membrane recovery is below 50%. An alternative to the membrane separation technique is the use of highly efficient emergent technology (photocatalyst material) to treat wastewater in the presence of solar irradiation. The use of nanomaterial as photocatalyst is on demand due to its unique feature of having a high surface area to volume. However, the direct application of nanomaterial in suspended form for

Editorial responsibility: J. Aravind.

✉ Z. Arif
zeenata.rs.che15@itbhu.ac.in

[1] Department of Chemical Engineering and Technology, Indian Institute of Technology (BHU), Varanasi, India

Table 1 List of conventional and emergent technologies for wastewater treatment: Pros and cons

Conventional/existing/emergent	Technology	Pros	Cons
Conventional	Chemical precipitation	Simple and inexpensive process High degree of selectivity Significant reduction in the chemical oxygen demand	Less efficient to treat water with high concentration of heavy metals Production of large volume of toxic sludge Handling and disposal problems (management, treatment, cost) Slow metal precipitation and sedimentation
Conventional	Coagulation-flocculation	Simple and inexpensive process Good sludge settling and dewatering characteristics Wide range of chemicals are available at low cost	Incomplete removal of heavy metals Precipitation method needs to be coupled to ensure effective removal Required non-reusable chemicals (coagulants, flocculants, aid chemicals)
Conventional	Adsorption	Relatively inexpensive and Simple operation Potential to separate a wide range of pollutants	Tedious process Requires regeneration and replacement which may be expensive and results in loss of material Rapid saturation and clogging affecting the efficiency of the reactors
Existing	Ion exchange	Technologically simple Rapid and efficient process Removal efficiency is very high	Sensitive to pH Requires large volume hence large columns is needed Easy fouling by particulates and organic matter. Efficient for removal of low metal concentration
Existing	Membrane filtration	Simple and highly efficient technique and requires small space High-quality treated effluent is produced No additional chemicals is required Minimal generation of solid waste	Maintenance and operational cost is high Feed wastage in form retentate High energy requirements
Emergent	Advanced oxidation processes	Little or no chemical consumption is needed Fast degradation Minimal volume of sludge production	Successful application at laboratory scale Formation of by-products Sensitive to pH

water treatments is inappropriate for recycling. From practical point of view, if the membrane surface is modified during synthesis procedure by incorporating photocatalyst material within the polymer matrix (Ramasundaram et al. 2016) to develop a hybrid material, coupling membrane separation and photocatalyst technology could present an integrated approach which not only eliminate Cr (VI) from wastewater but also reduce it to non-toxic Cr (III) form. Use of hybrid membrane (nanocomposite membrane), i.e., adding the highly photoactive nanomaterial (inorganic component) to the organic component led to their good performance. The use of nanocomposite membranes not only results in enhanced flux with high removal efficiency but also eliminates the fouling tendency of the membrane, increases the mechanical strength, thereby increasing the life span of membrane material (Nayak et al. 2016). At the same time, problem associated with poor recoverability of powdered material after treatment is also removed.

Polyvinylidene fluoride (PVDF) is a widely used polymer (organic component) for the ultrafiltration process because of its excellent resistivity against organic and inorganic acids and easy processability. However, being hydrophobic, the easy membrane fouling tendency affects the selective efficiency, and the chemical cleaning operations further increases its instability and deteriorates the sieving efficiency. The drawbacks can be eliminated by using different techniques including graft polymerization, chemical grafting, and surface coating membrane has been used to improve the surface hydrophilicity (Arif et al. 2019), but the weak interaction between polymer and additives affects the durability of the membrane (Salimi and Yousefi 2013). The incorporation of photocatalysis material into the polymer matrix is gaining interest. It is an effective approach to enhance membrane hydrophilicity, thereby improving the water flux and simultaneously antifouling and self-cleaning property (Mo et al. 2007). Among different types of nanoparticles existing, e.g., titanium dioxide (TiO_2) nanoparticles (NPs) (Yang and Wang 2006), Al_2O_3 (Yan et al. 2009), carbon nanotubes (Brunet et al. 2011), ZnO (Zhang et al. 2014), nano-sized TiO_2

is of high demand because of facile synthesis, excellent hydrophilicity and antibacterial property.

In this research, the effect of green route synthesized TiO_2 loading on PVDF membrane efficacy was evaluated. The novelty of this study involves the first time use of an extract of *Cajanus cajan* (obtained easily from kitchen waste thus avoiding the use of a costly chemical reducing agent) to synthesize NPs. The synthesized particle will be used as a filler to enhance the property of polymeric membrane used for ultrafiltration application in terms of porosity, pore size, thermal stability, flux and separation efficiency. The presence of active substance terpenoids, aliphatic, and aromatic amines (active substance) in extract result in efficient stabilization and avoid agglomeration of NPs. Most of the literature reported the removal of Cr (VI) either using either a membrane or photocatalytic removal technique. Using a membrane as such leads to increases in Cr (VI) concentration on the retentate site; hence, further treatment is required to treat it before discarding, thus increasing the operation cost. In case of using photocatalyst material, the additional cost occurs because of difficulty in the recovery of photocatalyst material after the treatment. This study also includes the application of synthesized nanocomposite membrane to be used as bi-functional membrane for ultrafiltration application. The bi-functional membrane will not only reject but also reduce Cr (VI) leading to the potential recovery of non-toxic Cr (III) using same inorganic-polymer material and retaining its efficiency even after several runs, thus reducing the processing cost. Thus the membrane performance was defined in terms of chromium (VI) rejection and subsequently to retreat the concentrated chromium (VI) called retentate at the end of the filtration process to remove toxicity by reducing Cr (VI) to Cr (III) a non-toxic element.

Materials and methods

Material

Polyvinylidene fluoride (PVDF) (average molecular weight $M_w = 534{,}000$ g/mol), a base polymer, n-methyl-2-pyrrolidone (NMP) as a solvent, was purchased from Sigma-Aldrich (Bombay). Titanium isopropoxide (TTIP) ($Ti[OCH(CH_3)_2]_4$), a precursor for TiO_2 synthesis, nutrient broth (NB) and nutrient agar (NA) used were obtained from High Media (Bombay). Double distilled water (DD) prepared in the laboratory was used in all experiments.

Synthesis TiO_2 nanoparticles (NPs)

Split and dehusked *Cajanus cajan* seeds (arhar pulse (dal)) were collected from the local market. The seeds were thoroughly washed firstly with clean tap water and then with distilled water (DD) to remove surface dust present. About 20 g of the cleaned washed seeds were soaked in 100-mL DD water beaker of borosilicate and was heated to 80 °C for 4 h. The obtained yellow color extract was filtered through a Whatman No-01 filter paper, collected and stored. One hundred eighty milliliters of 5 mM TTIP solution was prepared, followed by the addition of 60 ml collected pulse extract in the ratio of 18:6 (v/v). The mixture was stirred for 7 h without any heating. After 7 h, the precipitate formed at the bottom of the beaker was filtered and centrifuged using High-Speed Research Centrifuge-TC 4100 F at 10,000 rpm for 0.5 h to separate the powder from the extract. This step is followed thrice in order to remove the other unwanted material if present. The obtained yellow colored powder was dried at 100 °C overnight in an air oven followed by calcination at 570 °C in a muffle furnace for 3 h. The obtained white-colored TiO_2 NPs were then immobilized in a PVDF polymer matrix in known fixed amounts to obtain polymeric composite membranes with different TiO_2 loading.

Preparation of PVDF/TiO_2 composite membranes

The phase inversion technique was followed to synthesize PVDF composite membranes. Firstly, the PVDF pellets and synthesized TiO_2 NPs were dried in an oven at 90 °C for 4 h. Dried PVDF pellets (10 g) were then dissolved in NMP solvent (50 ml) and stirred on a magnetic stirrer at 70 °C for 0.5 h to achieve a homogeneous solution. In the meantime, a different amount of TiO_2 was taken and dispersed uniformly in 10 ml NMP using sonicator for half an hour. After 0.5 h, the uniformly prepared suspension of TiO_2 was mixed to the above prepared PVDF polymeric solution followed by continuous stirring for 10 h at 70 °C. The prepared casting solution was poured and cast as a film on a glass plate maintaining a clearance of 180 µm. The different cast film was exposed to air for 60 s for partial evaporation then placed in a water bath at temperature (28 ± 1 °C) for 24 h for immersion precipitation. The membranes were then peeled off, washed, and stored underwater for further analysis. Membranes incorporated with different loading of TiO_2 are designated as PM1 (0 wt % TiO_2), PM2 (0.1 wt % TiO_2), PM3 (0.2 wt % TiO_2), and PM4 (0.3 wt % TiO_2) (Arif et al. 2019). The experimental design of this study is depicted in Fig. 1 giving general description of the work done along with characterization technique used.

Characterization

X-ray diffractometer (XRD) Smart Lab X-ray diffractometer (Rigaku Smart Lab Powder type, without χ-cradle) was used to confirm the synthesis of TiO_2 NPs. It is operated at 18KW and consists of Rotating Anode XRD (1200–1800 K temperature, CuKα radiation of λ 1.5406 Å).

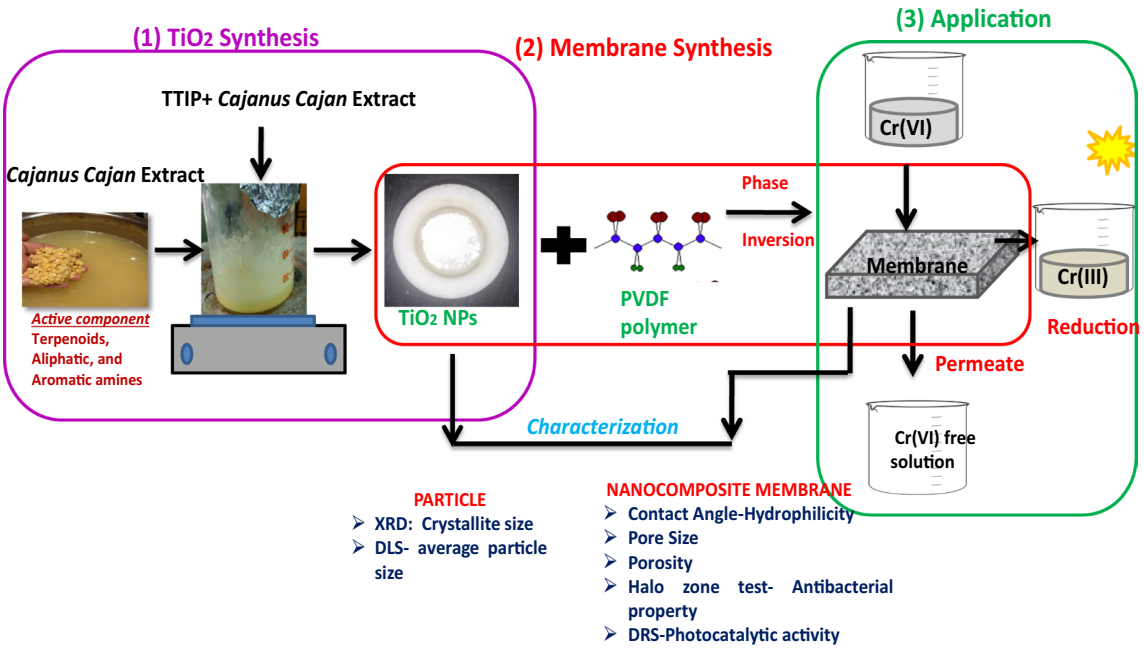

Fig. 1 Study design of the work

Particle size analyzer Nano Plus (zeta/nanosize analyzer) working on the principle of dynamic light scattering technique was used to define the average particle size.

Contact angle analyzer Wetting property of membrane was analyzed using contact angle goniometer [KRUSS, Germany] by sessile drop method using two µL DI water as probe liquid.

Thermo-gravimetric analysis (TGA) and differential scanning calorimetry (DSC) The thermal property of polymer composite membrane was analyzed using thermo-gravimetric analysis (TGA) and differential scanning calorimetry (DSC) using Perkin Elmer Simultaneous Thermal Analyzer STA 6000. The experiments were carried out in an N_2 environment (10 ml min^{-1}). The temperature ranged from 20 to 900 °C for TGA and 20 to 600 °C for DSC at a heating rate of 10 °C min^{-1}.

Fourier transform infrared spectra (FTIR) Fourier transform infrared spectra (FTIR) of nanocomposite film were recorded on TIR (02) [Perkin Elmer, Bruker] in the range of 500–4000 cm^{-1}.

Diffuse reflection spectrum (DRS) Studies for the Optical band gap were carried out using CARY-100 Bio UV–Visible spectrophotometer, wavelength ranging from 200 to 1000 nm.

Membrane porosity, tortuosity, and pore size

The gravimetric method was used to evaluate the membrane porosity (ε). The simple experiment was carried out where membranes were cut into small pieces of dimensions 0.01 m × 0.01 m and immersed in ethanol for 1 h. Before immersing their dry weight (W_d) was measured. After 1 h, the films were removed from the ethanol, and the surface was blotted with tissue paper; their wet weights were measured (W_w). The porosity was calculated (Roshani et al. 2018) using Eq. (1)

$$\varepsilon = W_w - W_d/(A \times l \times \rho) \tag{1}$$

where A, l, ρ represent membrane area (m^2) and m the thickness, and ethanol density is 789 kg m^{-3}, respectively.

Tortuosity (τ) shows an inverse relationship with porosity and could be calculated using Eq. (2)

$$\tau = \frac{(2-\varepsilon)^2}{\varepsilon} \tag{2}$$

Pore size (r) of the membrane was calculated using Eq. (3)

$$r_m = \sqrt{\frac{(2.9 - 1.7\varepsilon) \times 8\mu_w \times l \times Q}{\varepsilon \times A \times \Delta P}} \tag{3}$$

where μ_w is water viscosity (8.90×10^{-4} Pa s).

Thermodynamic and kinetic study

The incorporation of inorganic nanoparticles can improve the morphology and permeation property of the membrane. The presence of NPs in the polymeric solution induces the formation of smaller and run-through pores and suppresses the formation of macro-voids (Ya-nan et al. 2008).

In addition to it, they improve the porosity, permeability, and enhance the thermal stability and antifouling property.

In this work, the effect of synthesized TiO_2 NPs on the formation of the porous structure in poly(vinylidene fluoride) (PVDF)/N methyl pyrrolidone (NMP), solvent)/water (non-solvent) system via phase separation was investigated via immersion precipitation knowing that thermodynamics and kinetics are parameters are dependent on inorganic fillers. In the literature, two methods were reported to understand the kinetics of membrane fabrication, namely (i) the light transmission technique and (ii) the optical microscope technique (Kim and Lee 1998; Reuvers and Smolders 1987). It was concluded by Strathmann et al. (1975) that the square of distance moved by the boundary shows a linear relationship with coagulation time; therefore, Fickian diffusion law confirms the diffusion kinetics. Kang et al. (1991) further demonstrated the equation as

$$Y = 2\left(D_e t\right)^{1/2} \tag{4}$$

Squaring both sides in Eq. (4)

$$Y^2 = 4D_e t \tag{5}$$

where Y represent the distance moved by the boundary (mm), t the coagulation time (s), and D_e represents diffusion factor (mm^2/s)

In the membrane fabrication, the viscosity of the polymeric casting solution is an important parameter influencing the surface morphology and cross section of the membrane because it affects the exchange rate between solvent and non-solvent (Zheng et al. 2006). The viscosity test and cloud-point method were used to study the effect of incorporating synthesized TiO_2 NPs on the rheological and thermodynamic properties of PVDF casting solution, whereas the kinetic parameter was evaluated based on the relationship between the thickness of wet membrane and coagulation time.

Rheology and cloud-point measurement The rheological property was studied by measuring the viscosity of the polymeric solution, which was measured using Digital rotational viscometer (LMDV-60) at ambient temperature. The cloud point titration method was employed to study the thermodynamics of the casting solution. In this method, the polymer solution was titrated with water until the solution results in a cloudy feature. The titration was paused at first sight of turbidity, and the solution was shaken for 4-5 min to verify whether the solution remains turbid. If so, the cloud point measurement was achieved, and titration was stopped. The experiment was carried out in triplicate, and the average value was taken to minimize the experimental error.

Coagulation time and wet membrane thickness measurement The time was recorded after immersing the casting solution film into a coagulation bath to the moment it turned white indicates the demixing process is completed, and broke away from the glass plate is referred to as coagulation time and was measured using a stopwatch. The coagulation time will include diffusion between solvent and non-solvent across the membrane and the precipitation of polymer to finish demixing. Each experiment was carried out in triplicate, and the average value was taken to minimize the experimental error.

Antifouling test

Membrane fouling is one of the adverse drawbacks of using the pristine PVDF membrane as it lowers the efficacy of the membrane and life span. Thus, the antimicrobial activity of the synthesized PVDF/TiO_2 membranes was studied and compared with pure PVDF to understand the effect of the addition of TiO_2 NPs on the antifouling property of membranes. Two methods were reported in the literature to estimate the antibacterial activity: i) sterilization ratio calculation (Chong et al. 2017) and direct observation via FESEM (Chung et al. 2017). In this study, *E. coli* was used as the model foulant for the antimicrobial tests. Before the experiment, all the materials were autoclaved at 120 °C for 60 min to ensure sterility. *E. coli* was cultivated in a conical flask composed of 100 ml sterilized solution of nutrient broth kept in an incubator maintained at 37 °C for 1 day at 150 rpm to allow bacteria to grow fully. The overnight grown bacterial species were centrifuged for 15 min at 6000 rpm thrice to remove culture media and resuspended in sterilized DI water. UV-treated membrane pieces (0.01 m × 0.01 m) were taken and immersed in the cultivated *E. coli* suspension and placed in an incubator at 37 °C for 18 h. After that, the membranes were removed from the suspension, and 0.1 mL of the *E. coli* suspension was spread on an agar nutrient plate composed of 1.3 g of nutrient broth and 2.3 g of nutrient agar (NA) per 100 mL of distilled water and placed in the incubator for overnight. The number of colony-forming units (CFUs) on the plate was calculated using Eq. (6) which will determine the survival percentage of *E. coli* in the suspension

$$\text{Cell Viability}(\%) = N/N_o \times 100\% \tag{6}$$

where N and N_o represent colony count of *E. coli* suspension after immersion in PVDF/TiO_2 and pure PVDF (control) membrane; for direct observation method, the growth of *E. coli* on the membrane removed from the suspension was performed using HRSEM (high-resolution scanning electron microscope).

Rejection of Cr (VI) and photocatalytic reduction of Cr (VI)

The pristine PVDF and PVDF/TiO_2 membranes were used to carry out the rejection experiment in flow filtration cell

with the filtration area of 12.56 m^2. Then a chromium solution (Cr (VI), 8 mg/L, 200 ml) was passed through the membrane; the schematic representation of setup is shown in Fig. 1. The residual chromium concentration in permeation was estimated from the standard calibration curve (absorbance v/s concentration of Cr (VI)) at wavelength 350 nm, using a spectrophotometer (SYSTRONICS, PC Based Double Beam Spectrometer 2202). After 2 h, the concentrated chromium at the retentate side was collected in a 500-ml beaker consisting of the same membrane fixed at the bottom and subjected to photocatalytic degradation under sunlight. Ten-milliliter samples were collected at regular intervals and analyzed for Cr (VI). The schematic representation of the setup is shown in Fig. 2.

Results and discussion

Particle and membrane characterization

XRD

The formation of TiO_2 NPs was confirmed from the XRD patterns, as shown in Fig. 3a. The sharp diffraction peak intensity indicates the excellent crystalline structure. The diffraction peaks obtained at 2θ of 25.4°, 37.9°, 48.02°, 54.02°, 55.3°, 68.97° and 75.9 signifies the anatase phase of TiO_2 NPs, and corresponding Miller indices (hkl) values are (101), (004), (200), (105), (211), (116), (215). The obtained peaks match with peaks mentioned in JCPDS 21-1272, confirming the successful formation of TiO_2 NPs (Li et al. 2014). Debye–Scherrer's equation was used to calculate the crystalline size of the particle as

$$d = 0.89\lambda/\beta\cos\theta \tag{7}$$

where d represents crystalline size (nm), λ is the X-ray wavelength (0.154 nm), θ represents the Bragg's diffraction angle, and β is FWHM (full width at half maximum). The calculated crystalline size of the NPs was found to be 15.89 nm.

The average particle size distribution curve obtained from dynamic light scattering (DLS) technique is shown in Fig. 3b. The figure depicts the monodisperse distribution of particles with an average diameter ranging from 20 to 40 nm.

FTIR

The peaks corresponding to different groups in FTIR spectra are shown in Fig. 3c. The main conclusions drawn are that the presence of peak intensity of –OH groups is due to the presence of TiO_2 content in a polymer matrix, and peaks at wave number 640 cm^{-1} confirm the presence of NPs in PVDF/TiO_2 membrane (Wei et al. 2011). The other peaks in all membranes at wave number 3748, 1658, 1398, 1171 cm^{-1} correspond to the functional group –OH, H–O–H, C–H deformation, C–F stretching, respectively, whereas the peaks obtained at 640 cm^{-1} in PM2, PM3, PM4 correspond to Ti–O–Ti group thus confirming the presence of TiO_2 nanoparticle within the polymer matrix.

The β-phase ($F(\beta)$) and α-phase ($F(\alpha)$) content (%) in the PVDF/TiO_2 membrane were calculated using the Lambert–Beer law is given in Eq. (8)

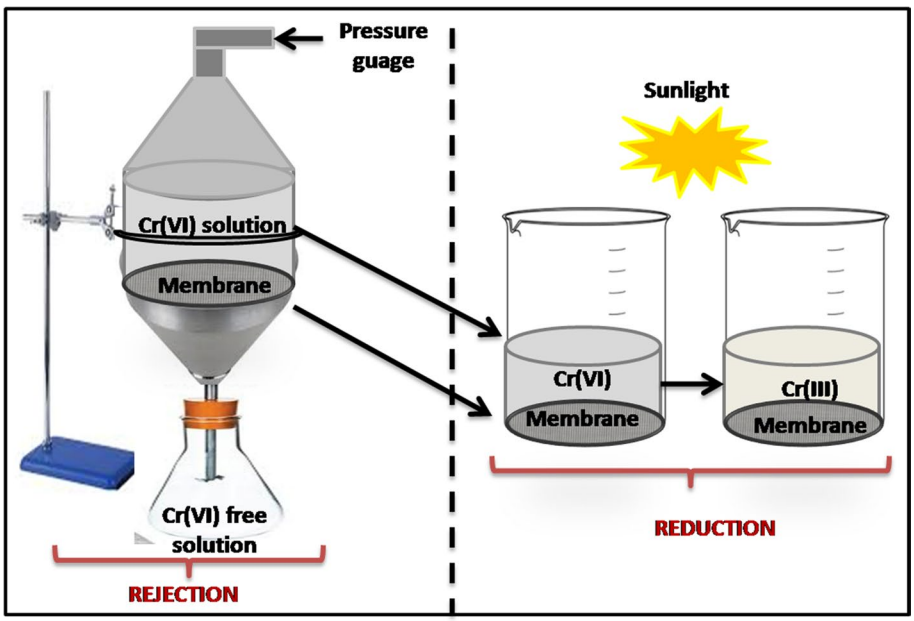

Fig. 2 Schematic representation for rejection and reduction experiment

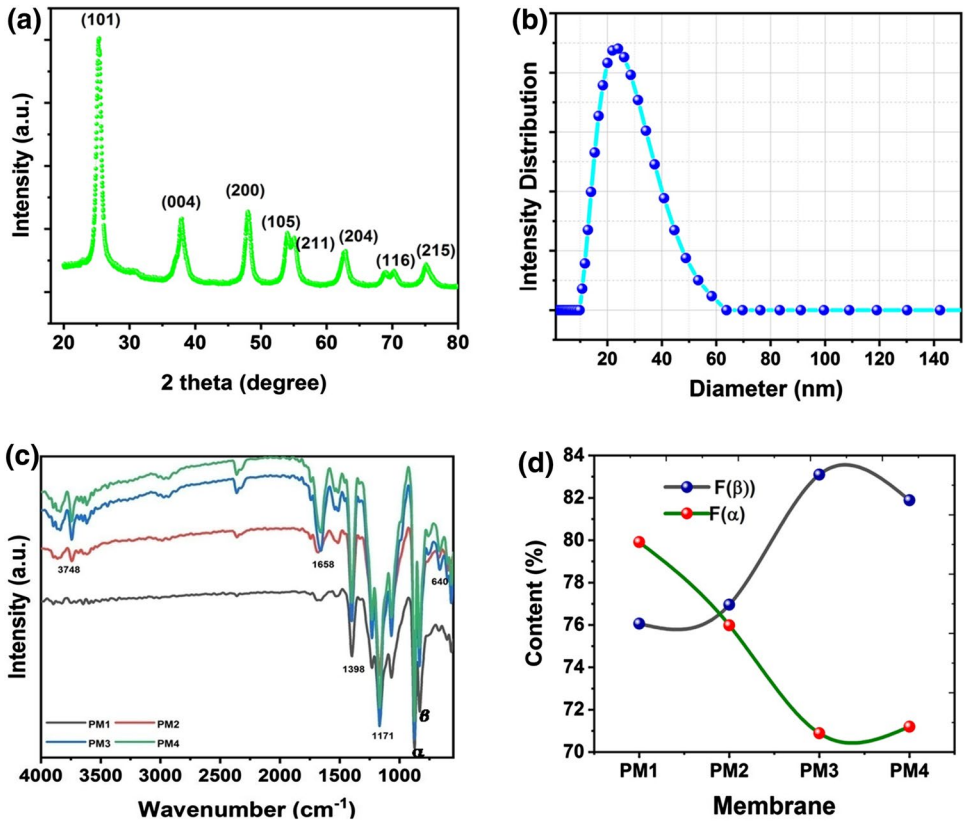

Fig. 3 **a** XRD pattern, **b** DLS spectra of synthesized TiO_2 NPs, **c** FTIR spectra and **d** Fraction value of α and β-phases of pure PVDF and PVDF/TiO_2 composite membranes

$$F(\beta) = \frac{a_\beta}{\frac{k_\beta}{k_\alpha}a_\alpha + a_\beta} \times 100 \text{ and } F(\alpha) = \frac{a_\alpha}{\frac{k_\alpha}{k_\beta}a_\beta + a_\alpha} \times 100 \quad (8)$$

where a_α and a_β refers to the absorbance value at wavelength 760 and 860 cm^{-1}, respectively, corresponding to α and β-phases (Vinoth et al. 2019). It was observed that the peak intensity corresponding to the α phase of PVDF diminished attributing to the addition of TiO_2 NPs. The β-phase content was calculated using Eq. 8. The calculated content of β-phase for pure PVDF and PVDF/TiO_2 is shown in Fig. 3d. The figure depicts that with increasing concentration of TiO_2 there is a shift from the crystalline α phase to β phase, and maximum was achieved for PM3 membrane due to the incorporation of TiO_2 NPs and also due to the interaction between polymer and inorganic filler (Vinoth et al. 2019) which is desirable because it has been reported in the literature that β phase is considered as the thermodynamically stable form which results in the enhancement of toughness in nanocomposite materials (Lai et al. 2014).

Thermogravimetric analysis (TGA)

The TGA results depict that the PVDF starts to decompose by thermally breaking of the –C–H bond (410 J mol^{-1}) and –C–F bond (460 J mol^{-1}) to form C–C double bonds, and the mass loss occurs due to the elimination of HF and scissoring of polymer chain along with the formation of tar (Wang et al. 2014). Figure 4a depicts that the membranes are thermally stable up to 300 °C and then degradation starts. The weight loss for the neat PVDF membrane (PM1) begins at 290 °C, and for PVDF/TiO_2, it starts from 450 °C. It was also observed that the thermal stability of the PVDF/TiO_2 is higher than the pure PVDF membrane and increases with an increase in the concentration of NPs. The significant weight loss was observed in the range from 400 to 500 °C which is assigned to the degradation of PVDF polymer. The weight loss decreases with an increase in TiO_2 loading attributed to the interaction of TiO_2 with the polymer matrix, and this interaction leads to delay in the diffusion of the volatile compound out of the polymer thereby enhancing the thermal decomposition temperature (defined as the temperature at 3–4% weight loss). Similar results were also reported in the literature (Shi et al.2013). For all nanocomposite membranes, a non-combustible residue that ensures the presence of the inorganic component (TiO_2) was left behind.

Differential scanning calorimetry (DSC)

The thermal property of membranes was also analyzed using differential scanning calorimetry (DSC). Figure 3b represents an endothermic peak in DSC chromatograms.

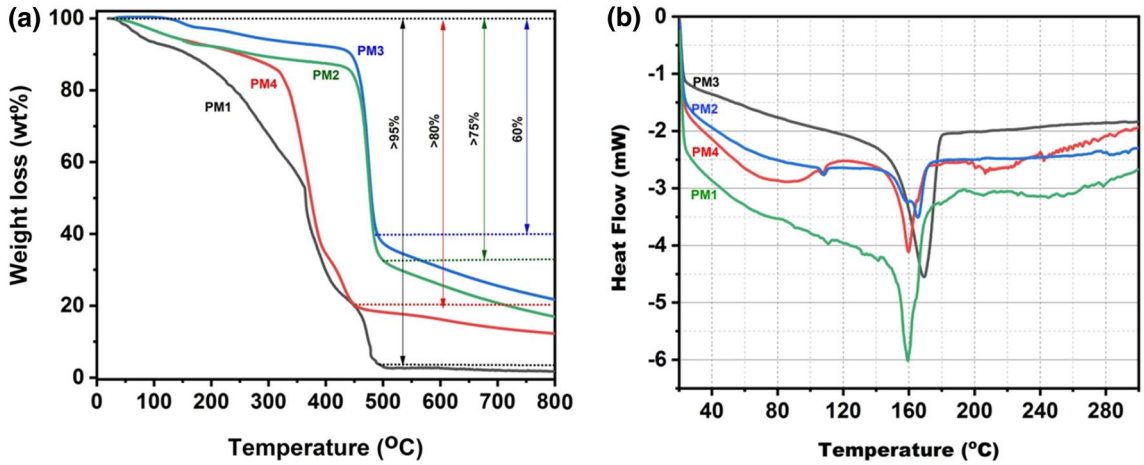

Fig. 4 **a** TGA curve, **b** DSC curve of pure PVDF and PVDF/TiO_2 composite membranes

The figure revealed melting temperature of pure PVDF is 159.04 °C, whereas for nanocomposite membrane it shifted toward right and increases to 165.69 °C for PM2, 169.96 °C for PM3 and 161.02 °C for PM4. This increment is due to the excellent thermal property of TiO_2 which will obstruct the decomposition of the polymer matrix by enhancing the rigidity in the PVDF chain. The interaction between the macromolecular chain of the polymer and TiO_2 will restrain the state of PVDF chains, resulting in increases in the rigidity of polymer chains and restricting their thermal action; hence, the melting temperature of the composite membrane increases. The decreased value in the case of PM4 is due to agglomeration of a particle at high concentration reducing the surface-to-volume ratio; hence, contribution of interfacial effects will hinder the thermal characteristics (Nor et al. 2016).

Optical band gap analysis

Figure 5a shows the UV–Vis spectra of PVDF and PVDF/TiO_2 membranes. The figure depicts that absorption capability of pure PVDF is minimal, as it did not absorb any light in the range 200 to 500 nm compared to TiO_2 incorporated membranes toward UV radiation which indicates an excellent optical response of PVDF/TiO_2 membranes to UV irradiation (Nor et al. 2016). This is attributed to nanoparticle-polymer ionic interaction (Sharma et al. 2018). The corresponding band gap (difference of conduction and valence band energy and a significant parameter for a photocatalytic reaction to happen) energy was calculated using Kubelka–Munk function (Escobedo Morales et al. 2007), and the Tauc plot ($\alpha h\nu^2$ versus the energy for direct transition) was used to evaluate the band gap energy of the prepared composite membranes using Eq. (9)

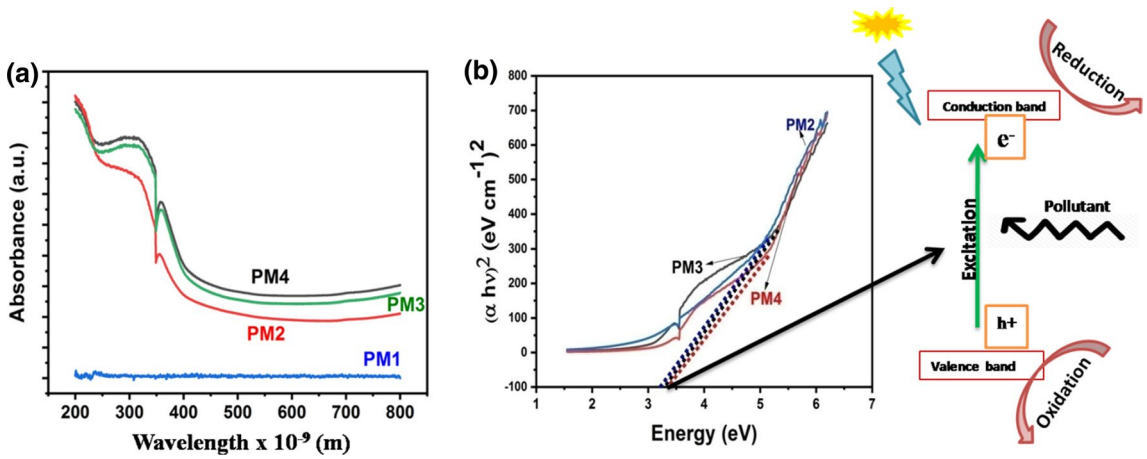

Fig. 5 **a** DRS spectrum, **b** band energy of PVDF/TiO_2 composite membranes

$$(\alpha h\nu)^n = A(h_\nu - E_g) \quad (9)$$

where α, h, ν and E_g represent absorption coefficient, Planck constant (6.63×10^{-34} J s), speed of light (3×10^8 m s $^{-1}$), and band gap energy, respectively, n characterizes the nature of the transition process, i.e., n = 2 indicates the direct transition.

The calculated values of the band gap are 3.31, 3.52, and 3.59 eV for PM2, PM3, and PM4 membrane, respectively, as shown in Fig. 4b. It was observed that the value of band gap energy is higher than TiO_2 NPs (3.2 eV) due to the uniform distribution of NPs within the polymer matrix. These results suggest that the pure PVDF membranes act as support for electron transport (Wang et al. 2017).

PVDF/TiO_2 composite membrane–thermodynamic approach

Cloud point plot The cloud point plot at different loading of TiO_2 is shown in Fig. 6a. The figure depicts that with increasing TiO_2 loading, the cloud point curve shifts toward the solvent axis gradually. It suggests that the solvent has a good affinity toward TiO_2 and may form a hydrogen bond, thereby weakening the affinity between PVDF and solvent, intensifying the aggregation of PVDF macromolecules, and increasing the demixing rate. It indicates that the addition of TiO_2 favors the demixing of casting solution thermodynamically.

PVDF/TiO_2 composite membrane—kinetics approach

The relation between wet membrane thickness and coagulation time was used to investigate the kinetics of the

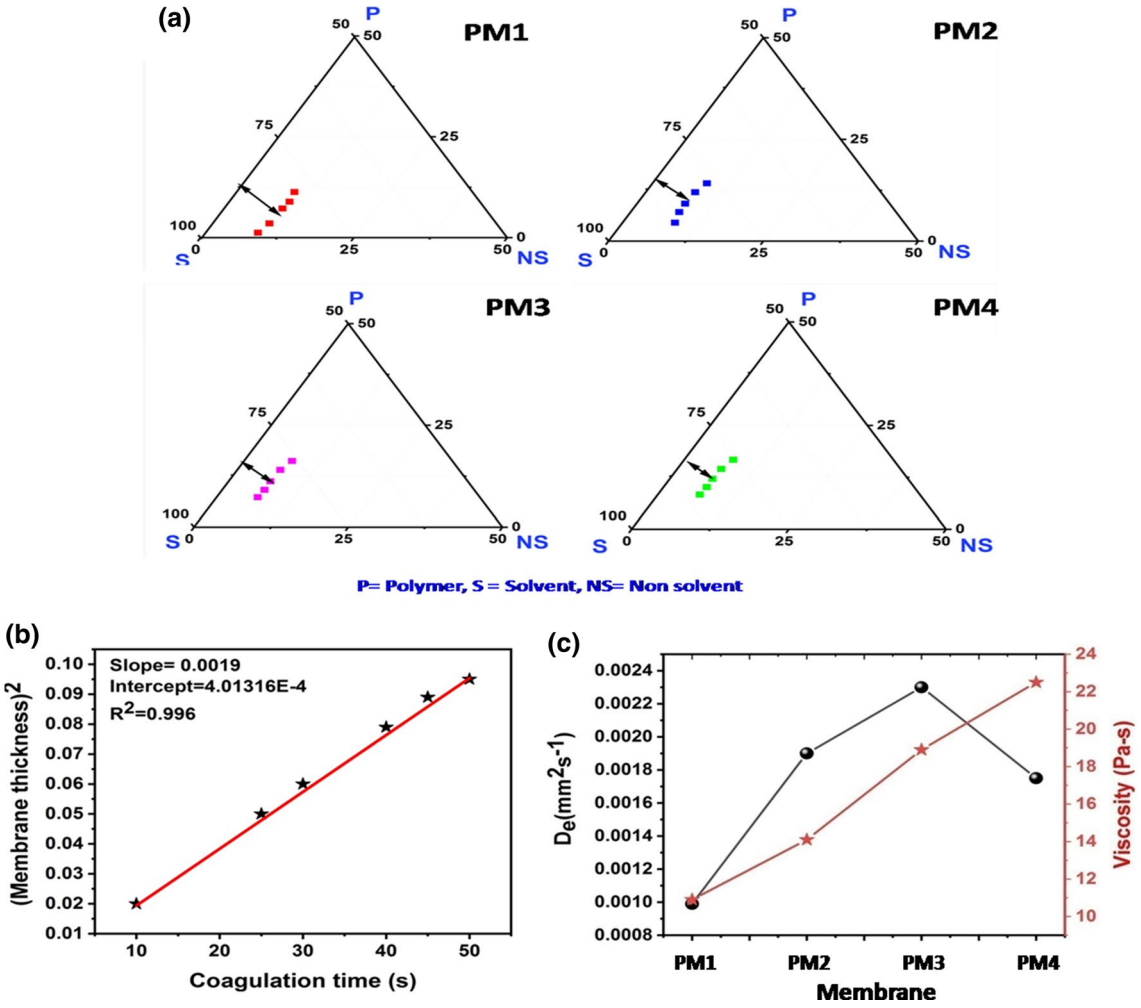

Fig. 6 **a** Ternary phase diagram of PVDF/TiO_2 at different TiO_2 loading, **b** plot between the square of membrane thickness and coagulation time for PM3 membrane, **c** D_e and viscosity of casting solution with respect to TiO_2 loading

synthesized PVDF/TiO_2 membrane. The membrane of different thickness was fabricated by adjusting the clearance between the casting knife and glass plate and the stopwatch used to record the coagulation time at ambient temperature. The plot between the square of membrane thickness and coagulation time and its regression analysis is as shown in Fig. 6b, and its error analysis detail is given in Table 2. The figure depicts a linear relationship between coagulation time and the square of wet membrane thickness.

The line equation can be written as Eq. (10)

$$Y^2 = 4.01316 \times 10^{-4} + 0.0019t \quad (10)$$

Since the coagulation time was always more than 10 s, the intercept (4.01316×10^{-4}) always less than 1% can be neglected, and the equation can be rewritten as

$$Y^2 = 0.0019t \quad (11)$$

Comparing Eqs. (5) and (11)

$$Y^2 = D_e t$$

$$D_e = Y^2/t$$

where Y represents the membrane thickness (mm), t coagulation time (s), D_e kinetic parameter ($mm^2\ s^{-1}$), defined as diffusing rate of solvent and non-solvent. Similarly, D_e value for other PVDF/TiO_2 membranes was calculated. It was well known that the composition of the casting solution strongly influences the kinetics of the membrane. At constant coagulation bath temperature, the solution viscosity increases with increasing concentration of TiO_2; however, D_e value rises up to TiO_2 loading 0.02 wt % and maximum value of 0.023 $mm^2\ s^{-1}$ for PM3 membrane was achieved, and then, D_e value decreases on the further increase. The change in D_e with the TiO_2 concentration was due to thermodynamic and rheological properties. The addition of TiO_2 enhances the thermodynamic property due to an increased demixing rate. But at maximum loading (PM4-0.3 wt % TiO_2), the increased viscosity creates a negative impact on D_e because of the increased viscosity slows down the exchange rate.

Table 2 Error analysis for plot between the square of membrane thickness and coagulation time

Intercept		Slope		Statistics
Value	Standard error	Value	Standard error	Adj. R-square
4.01316E−4	0.00174	0.0019	4.86629E−5	0.99607

Thus, it can be said that the rheological factor decreases D_e. Hence it can be concluded that the thermodynamic and the rheological factor show a trade-off relationship against one another. At low TiO_2 concentration, the thermodynamic property becomes dominant, and at high concentration, rheological hindrance becomes prominent and influences the kinetics of membrane formation (Ya-nan et al. 2008). The trend of D_e and viscosity of PVDF/TiO_2 hybrid membranes is shown in Fig. 6c.

Contact angle, pore size, porosity, tortuosity

The contact angle values determine the hydrophobicity of the membranes. Figure 7a depicts that the observed contact angle of PVDF/TiO_2 membranes is lower than the neat PVDF membrane. It is due to a high hydrophilic characteristic of TiO_2 NPs. It was observed that the contact angle value declines from 94.9 to 77.2° as TiO_2 loadings increase from 0 to 0.3 wt %. Similar results were also reported by Arif et al. (2019). These results suggest that hydrophilicity is improved for the PVDF/TiO_2 composite. The opposite trend to contact angle for porosity and pore size was observed (Fig. 7b, c). The porosity increases from approx. 74 to 85%, and the difference in porosity for PM1 and PM2 is more tangible compared to PM3 and PM4. It is due to a decrease in the rate of increasing porosity due to increased viscosity of the solution, which reduces the exchange of mass transfer rate between solvent and non-solvent, thus reducing the porosity and hence the pore size, with increasing inorganic TiO_2 concentration. The results were supported by the kinetic study also. As already mentioned that inverse relationship exists between tortuosity and porosity. Figure 7d also shows a similar trend where tortuosity decreases with an increase in TiO_2 loadings.

Antifouling test

The calculated cell viability and bacteria growth are shown in Fig. 8a–c. Figure 8 b shows the growth of *E. coli* on NA plates after 24-h incubation. The figure depicts that there was an abundance growth of *E. coli* in the case of PM1 (control). On the other hand, TiO_2-incorporated membrane viability of *E. coli* was very less compare to pure PVDF, and in the case of PM3 and PM4, there was hardly any growth of *E. coli* on the plates. These results suggest that the sterilization effect of the membranes was excellent. The HRSEM images confirm the antimicrobial activity of the membranes. A shown in Fig. 8c, a dense layer of *E. coli* was observed on the surface of pure PVDF, which is not the case with TiO_2

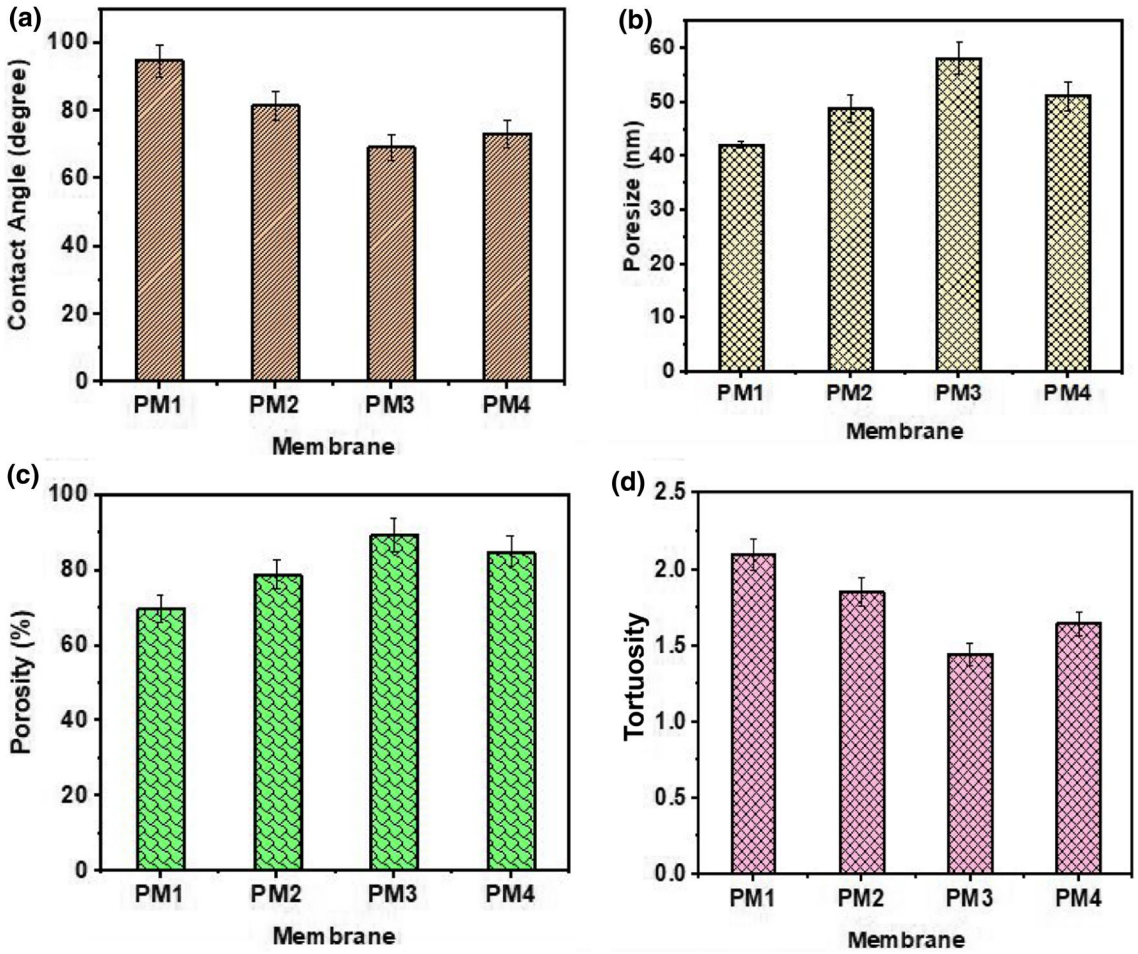

Fig. 7 **a** Contact angle, **b** pore size, **c** porosity, **d** tortuosity of the different composite membrane

incorporated PVDF membrane, and a significant antimicrobial efficacy was observed with increasing TiO_2 loading. It is attributed to the cell wall disruption due to the presence of NPs (Belay 2010). At low concentration, for the PM2 membrane, the surface was not entirely covered with NPs, therefore, allowing few bacteria to grow. In the case of PM3, the optimum loading results in intimate contact between TiO_2 NPs and the bacteria but further increase in loading (PM4); the agglomeration of particles leads to non-uniform distribution within the polymer matrix hence provides a surface for bacteria to grow.

Rejection of Cr (VI)

Figure 9a shows that with increasing TiO_2 loading water, flux increases. It is due to the incorporation of hydrophilic TiO_2 NPs and increased porosity, as shown in Fig. 7a, c also, but for the PM4 membrane, the flux declines due to decreased porosity attributed to delayed mixing rate with increased viscosity, which is also justified from the results shown in Fig. 6c. Figure 9b depicts the % rejection for feed solution containing Cr (VI) for different membranes. It was observed that % rejection was very less for pure PVDF membrane and increased with an increase in TiO_2 loading, and nearly 85.59% chromium rejection was achieved. It is mentioned in various literature that separations are influenced by the presence of charge on the membrane, the concentration of solute, ionic interaction of inorganic filler with the membrane (Jyothi et al. 2017). Here the chromium removal is due to strong electrostatic interaction between TiO_2 and Cr ions as Cr exists in its anionic form ($Cr_2O_7^{2-}$,CrO_4^{2-} and $HCrO^{4-}$), and amphoteric nature of TiO_2 induces a positive charge (Ti-OH_2^+) on the membrane surface at acidic pH (6.1) (Jyothi et al. 2017; Kazemi et al. 2018). Hence, positively charged membrane will repel the cation and can adsorb the mentioned anions; hence, rejection occurs, which is not the case with pure PVDF membrane. The increased % rejection with increasing loading is due to increased surface charge of on the membrane; also the presence of hydrophilic TiO_2

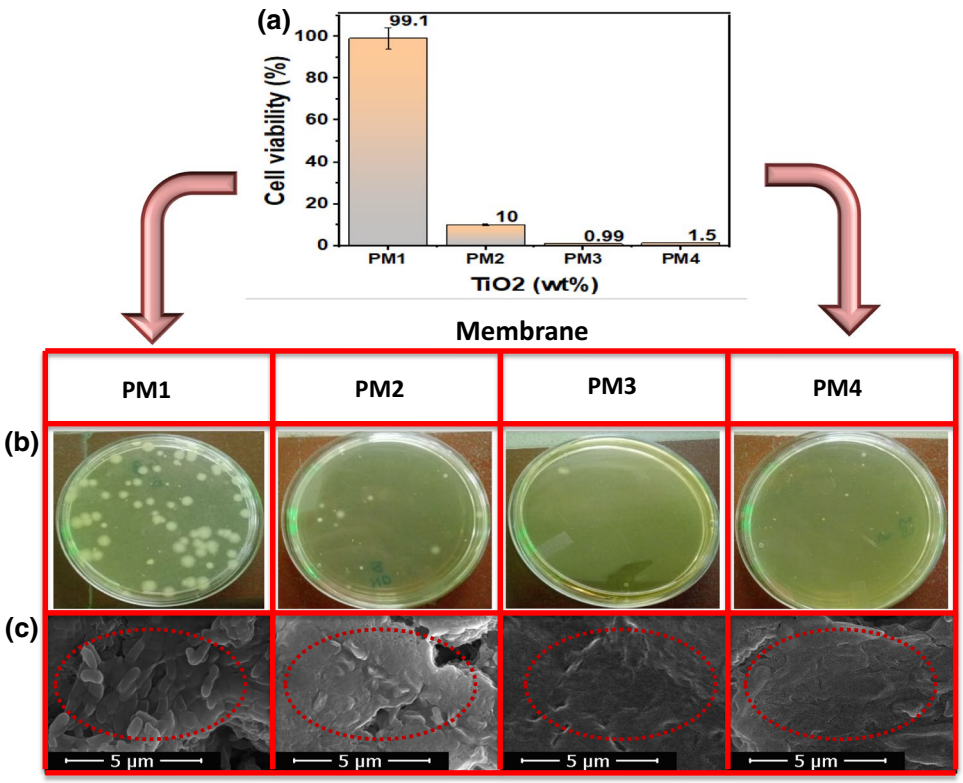

Fig. 8 **a** Cell viability, **b** *E. coli* colonies on NA plate, **c** HRSEM images of the surface of the membrane

NPs increases water flux but further increase in loading in case of PM4 membrane excess loading creates negative impact the on rejection percentage due to widening of pores (sponge-like pores) as mentioned in an earlier section and will also lower the flux due pore plugging and hinder diffusion (Jyothi et al. 2017).

Reduction of Cr (VI) to (III)

It was observed that with time, the Cr (VI) concentration increases in the feed side up to 13.8 ppm. Now the feed solution is subjected to photo-catalytic degradation. The % reduction profile for the different membranes is shown in Fig. 9b; a maximum of 92% reduction was observed within 60 min at acidic pH (6.1) for the PM3 membrane. It is attributed to the generation of electrons into the interface of the polymer when illuminated with light leading to electron availability for Cr (VI) reduction. The electrons will be utilized by Cr (VI) to get reduced to Cr (III), where the acid environment will oxidize the hole produced in the valence band, thus avoiding the recombination possibility also (Jyothi et al. 2017). However, in the case of pure PVDF, the small change observed may be attributed to the adsorption phenomenon.

The complete electron transfer steps are shown in Scheme 1 (Jyothi et al. 2017).

Here the Cr (VI) ions in acidic medium undergo complete dissociation and can be reduced to Cr (III). Comparatively, the proposed method of synthesizing bi-functional membrane to obtain simultaneous improved rejection and reduction which is cost-effective in terms of less time consumption and excellent selectivity (Scheme 2).

The reusability without affecting its efficiency is a significant parameter deciding the potential of the product. Among the synthesized membranes, the PM3 membrane was used to test the reusability (both for rejection and reduction) based on its excellent performance. The experiment was run 5 times, and the results are summarized in Fig. 8c. The figure depicts that the membrane without a significant change retains its reusable capacity, but at the end of the 5th cycle, the PM3 membrane loses its strength due to applied pressure during separation hence was not used further.

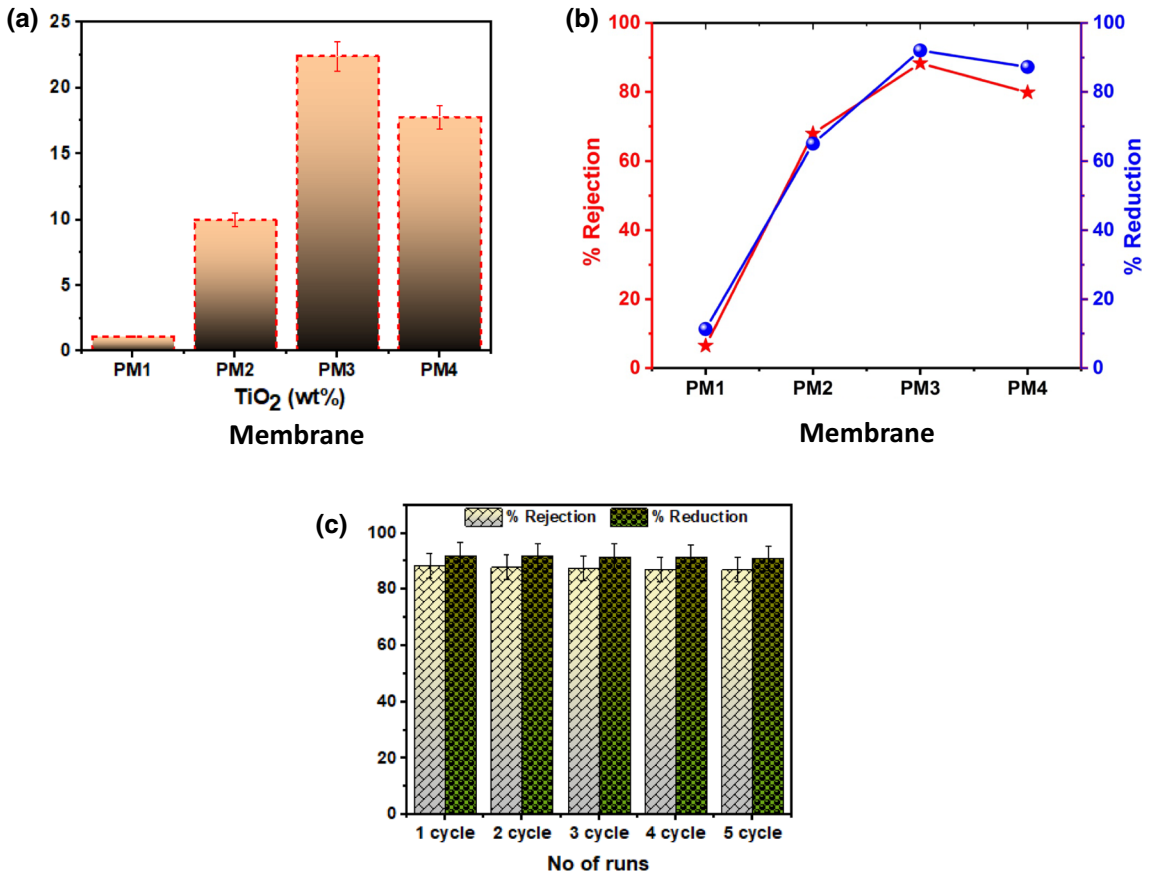

Fig. 9 **a** Water flux for different membrane, **b** rejection and reduction % of Cr (VI) at different TiO_2 loading, **c** Reusability of PM3 membrane for Cr (VI) removal

$$TiOH_2^+ + Cr_2O_7^{2-} \rightarrow TiOH.Cr_2O_7^{2-} + H^+$$

Scheme 1 The reaction between the catalyst and the reductant in acidic media

$$Cr(VI) \xrightarrow{e^-} Cr(V) \xrightarrow{e^-} Cr(IV) \xrightarrow{e^-} Cr(III)$$

Scheme 2 Steps for Cr (VI) reduction to Cr (III)

Hence, it can now be concluded that PVDF/TiO_2 immobilized membranes can be effectively used to remove chromium from wastewater. Also, after deep investigation, a comparative analysis is carried out to compare the efficiency of other used techniques with the synthesized membrane in this work as listed in Table 3. It is seen that the bi-functional membrane presents a promising approach with different techniques. Compared to other technique reported in the literature, the % removal is maximum at pH ~6 without much compromising in removal efficiency even after 5 runs and almost achieving best result when compared to commercial available expensive membrane technique (nanofiltration (NF) and reverse osmosis (RO), and this may broaden the horizon for treatment of tannery wastewater using bi-functional membrane technology.

Conclusion

Anatase phase TiO_2 of crystalline size 15.89 nm was successfully synthesized using *Cajanus cajan* seed extract. The synthesized TiO_2 NPs of different loading were incorporated in PVDF polymer matrix to demonstrate a bi-functional product that can be utilized as a membrane

Table 3 Comparison of the performance of nanocomposite membranes fabricated in this work and other technique reported in the literature

Material	Synthesized/commercial	%Removal	Process	References
Polyamide skin over polysulfone support—nanofiltration (NF) and polyamide—reverse osmosis (RO)	Commercial membrane	Approx 97% Cr removal	NF followed by RO process	Das et al. (2006)
Graphene oxide (GO) and polyaniline (PANI)	Synthesized particle	Approx 68% Cr removal	Adsorption	Shaban et al. (2018)
PSf/TiO_2 (0.4 g TiO_2)	Synthesized membrane	Up to 60% Cr removal	Membrane	Jyothi et al. (2017)
Amine-impregnated TiO_2nanoparticles-modified cellulose acetate membranes	Synthesized membrane	72.4% Cr removal at pH ~7	Ultrafiltration membrane	AlebelGebru and Das (2018)
Graphene oxide and polyaniline	Synthesized	The removal efficiency increases from 31.6 to 66.2% when GO dose increases from 25 to 150 mg	Adsorption	Shaban et al. (2018)
BiOBr (photocatalyst)/polytetrafluoroethylene (membrane)	Synthesized photocatalyst	Synergistic removal of 4-CP and Ag + ions.		Zou et al. (2020)
CMX/TiO_2	Commercial membrane	Removal of almost 95% for Cr (VI)	Ionic exchange membrane	Hsu et al. (2011)
Palladium nanoparticles supported on amine-functionalized SiO_2	Synthesized	Catalytic activity > 85% after the 5th catalytic reuse at room temperature	Catalytic reduction	Celebi et al. (2016)
PVDF/TiO_2 membrane (0.2 wt % TiO_2)	Synthesized bi-functional membrane	Approx 92% Cr removal at pH ~6.1 % removal reduces to 91% approx on 5 run	Membrane + photocatalyst	This work

to reject Cr (VI) and photo-catalyst to reduce Cr (VI) to non-toxic element Cr (III) which highlights its uniqueness using the same material as membrane and photocatalyst material. The effect of different loading TiO_2 results concludes that at optimal loading TiO_2 (PM3- 0.02 wt %) maximum rejection of 85.59% and reduction 92% was achieved. The influence of TiO_2 on membrane morphology was also studied by investigating the thermodynamic and kinetic parameters. It was concluded that thermodynamic enhancement accelerated the phase separation with increasing TiO_2 loading, thereby enhancing the porosity and water flux, but at maximum loading (PM4-0.03 wt %) the rheological hinderance becomes more prominent due to increased viscosity hence delaying the mixing rate and reducing the pore size formation; thus, there exists a trade-off relation between thermodynamic and kinetic parameter.

Acknowledgments The author would like to acknowledge the Central Instrument Facility (CIF) IIT(BHU) for TGA, DSC, and FTIR facility.

Compliance with ethical standards

Conflict of interest The authors declare "no conflict of interest in this publication.

References

Abdullah N, Yusof N, Lau WJ, Jaafar J, Ismail AF (2019) Recent trends of heavy metal removal from water/wastewater by membrane technologies. J Ind Eng Chem 76:17–38

Arif Z, Sethy NK, Kumari L, Mishra PK, Verma B (2019) Antifouling behaviour of PVDF/TiO_2 composite membrane: a quantitative and qualitative assessment. Iran Polym J 28:301–312

Belay A (2010) Impacts of chromium from tannery effluent and evaluation of alternative treatment. J Environ Prot 1:53–58

Brunet P, Lyon DY, Zodro K, Rouch JC, Caussat B, Serp P, Remigy JC, Wiesner MR, Chang S (2011) Application of submerged hollow fiber membrane in membrane bioreactors: filtration principles, operation, and membrane fouling. Desalination 283:31–39

Burakov AE, Galunin EV, Burakova IV, Kucherova AE, Agarwal S, Tkachev AG et al (2018) Adsorption of heavy metals on conventional and nanostructured materials for wastewater treatment purposes: a review. Ecotoxicol Environ Saf 148:702–712

Celebi M, Yurderi M, Bulut A, Kaya M, Zahmakiran M (2016) Palladium nanoparticles supported on amine-functionalized SiO_2 for the catalytic hexavalent chromium reduction. Appl Catals B: Environ 180:53–64

Chong WC, Mahmoudi E, Chung YT, Koo CH, Mohammad AW, Kamarudin KF (2017) Improving performance in algal organic matter filtration using polyvinylidene fluoride–graphene oxide nanohybrid membranes. Alg Res 27:32–42

Chung YT, Mahmoudi E, Mohammad AW, Benamor A, Johnson D, Hilal N (2017) Development of polysulfone-nanohybrid membranes using ZnO-GO composite for enhanced antifouling and antibacterial control. Desalination 402:123–132

Crini G, Lichtfouse E (2019) Advantages and disadvantages of techniques used for wastewater treatment. Environ Chem Lett 17:145–155

Das C, Patel P, De S, DasGupta S (2006) Treatment of tanning effluent using nanofiltration followed by reverse osmosis. Sep Purif Technol 50:291–299

Dhala B, Thatoib HN, Dasc NN, Pandey BD (2013) Chemical and microbial remediation of hexavalent chromium from contaminated soil and mining/metallurgical solid waste: a review. J Hazard Mater 250–251:272–291

Escobedo Morales UPA, Sanchez Mora E, Morales A, Mora E, Pal U (2007) Use of diffuse reflectance spectroscopy for optical characterization of un-supported nanostructures. Revista Mexicana de Física 53:18–22

Gebru KA, Das C (2018) Removal of chromium (VI) ions from aqueous solutions using amine-impregnated TiO_2 nanoparticles modified cellulose acetate membranes. Chemosphere 191:673–684

Hsu H-T, Chen S-S, Chen Y-S (2011) Removal of chromium (VI) and naphthalene sulfonate from textile wastewater by photocatalysis combining ionic exchange membrane processes. Sep Purif Technol 80:663–669

Jyothi MS, Nayak V, Padaki M, Balakrishna RG, Soontarapa K (2017) Eco-friendly membrane process and product development for complete elimination of chromium toxicity in wastewater. J Hazard Mater 332:112–123

Kang YS, Kim HJ, Kim UY (1991) Asymmetric membrane formation via immersion precipitation method. I. kinematic effect. J Membr Sci 60:219–232

Kazemi M, Jahanshahi M, Peyravi M (2018) Hexavalent chromium removal by multilayer membrane assisted by photocatalytic couple nanoparticle from both permeate and retentate. J Hazard Mater 344:12–22

Kim JH, Lee KH (1998) Effect of PEG additive on membrane formation by inversion. J Membr Sci 138:153–163

Lai CY, Groth A, Gray S, Duke M (2014) Preparation and characterization of poly(vinylidenefluoride)/nanoclay nanocomposite flat sheet membranes for abrasion resistance. Wat Res 57:56–66

Li W, Liang R, Hu A, Huang Z, Zhau YN (2014) Generation of oxygen vacancies in visible light activated one-dimensional iodine TiO_2 photocatalysts. RSC Adv 4:36959–36966

Loryuenyong V, Jarunsak N, Chuangchai T, Bua A (2014) The Photocatalytic Reduction of Hexavalent Chromium by Controllable Mesoporous Anatase TiO_2 Nanoparticles Adv Mater Sci Eng http://dx.doi.org/10.1155/2014/348427

Mo J, Son SH, Jegal J, Kim J, Lee YH (2007) Preparation and characterization of polyamide nanofiltration composite membranes with TiO_2 layers chemically connected to the membrane surface. J Appl Polym Sci 105:1267–1274

Nayak V, Jyothi MS, Balakrishna G, Padaki M, Isloor AM (2016) Synthesis and characterization of novel sulfanilic acid-poly vinyl chloride – polysulfone blend membranes for metal ion rejection. RSC Adv. 6:25492–25502

Nor NAM, Jaafar J, Ismail AF, Mohamed MA, Rahman MA, Othman MHD, Lau WJ, Yusof N (2016) Preparation and performance of PVDF-based nanocomposite membrane consisting of TiO_2 nanofibers for organic pollutant decomposition in wastewater under UV irradiation. Desalination 391:89–97

Ramasundaram S, Seid MG, Choe JW, Kim EJ, Chung YC, Cho K, Lee C, Hong SW (2016) Highly reusable TiO_2 nanoparticle photocatalyst by direct immobilization on steel mesh via PVDF coating, electrospraying, and thermal fixation. Chem Eng J 306:344–351

Reuvers AJ, Smolders CA (1987) Formation of membranes by means of immersion precipitation. Part II. The mechanism of formation of membranes prepared from the system cellulose acetate–acetone-water. J Membr Sci 34:67–86

Roshani R, Ardeshiri F, Peyravi M, Jahanshahi M (2018) Highly permeable PVDF membrane with PS/ZnO nanocomposite incorporated for distillation process. RSC Adv 8:23499–23515

Salimi A, Yousefi AA (2013) Analysis method: FTIR studies of β-phase crystal formation in stretched PVDF films. Polym Test 22:699–704

Shaban M, Abukhadra MR, Rabia M, Elkader YA, El–Halim MR (2018) Investigation the adsorption properties of graphene oxide and polyaniline nano/micro structures for efficient removal of toxic Cr (VI) contaminants from aqueous solutions; kinetic and equilibrium studies. *Rendiconti Lincei-Scienze Fisiche* 29:141–154

Sharma M, Quamara JK, Gaur A (2018) Behaviour of multiphase PVDF in $(1-x)$PVDF/$(x)BaTiO_3$ nanocomposite films: structural, optical, dielectric and ferroelectric properties. J Mater Sci: Mater Electron 29:10875–10884

Shi N, Duan J, Su J, Huang F, Xue W, Zheng C, Qian Y, Chen S, Xie L, Huang W (2013) Crystal polymorphism and enhanced dielectric performance of composite nanofibers of poly(vinylidene fluoride) with silver nanoparticles. J Appl Polym Sci 128:1004–1010

Strathmann H, Kock K, Amar P, Baker RW (1975) The formation mechanism of asymmetric membranes. Desalination 16:179–203

Vinoth S, Kanimozhi G, Kumar H, Srinadhu ES, Satyanarayana N (2019) High conducting nanocomposite electrospun PVDF-HFP/TiO_2 quasi-solid electrolyte for dye-sensitized solar cell. J Mater Sci: Mater Electron 30:1199–1213

Wang Q, Wang Z, Zhang J, Wang J, Wu Z (2014) Antifouling behaviours of PVDF/nano-TiO_2 composite membranes revealed by surface energetics and quartz crystal microbalance monitoring. RSC Adv 4:43590–43598

Wang C, Wu Y, Lu J, Zhao J, Cui J, Wu X, Yan Y, Huo P (2017) Bioinspired synthesis of photocatalytic nanocomposite membranes based on synergy of Au-TiO_2 and polydopamine for degradation of tetracycline under visible light. ACS Appl Mater Interf 9:23687–23697

Wei Y, Chu H, Dong B, Li X, Xia S, Qiang Z (2011) Effect of TiO_2 nanowire addition on PVDF ultrafiltration membrane performance. Desalination 272:90–97

Yan L, Hong S, Li ML, Li YS (2009) Application of the Al_2O_3–PVDF nanocomposite tubular ultrafiltration (UF) membrane for oily wastewater treatment and its antifouling research. Sep Purif Technol 66:347–352

Ya-nan Y, Jun W, Qing-zhu Z, Xue-si C, Hui-xuan Z (2008) The research of rheology and thermodynamics of organic–inorganic hybrid membrane during the membrane formation. J Membr Sci 311:200–220

Yang YN, Wang P (2006) Preparation and characterizations of new PS/TiO_2 hybrid membranes by sol–gel process. Polymer 47:2683–2688

Zhang X, Wang Y, Liu Y, Xu J, Han Y, Xu X (2014) Preparation, performances of PVDF/ZnO hybrid membranes and their applications in the removal of copper ions. Appl Surf Sci 316:333–340

Zheng Q-Z, Wang P, Yang Y-N (2006) Rheological and thermodynamic variation in polysulfone solution by PEG introduction and its effect on kinetics of membrane formation via phase-inversion process J Membr Sci 279:230–237

Zou Q, Zhang Z, Li H, Pei W, Ding M, Xie Z, Huo Y, Li H (2020) Synergistic removal of organic pollutant and metal ions in photocatalysis-membrane distillation system. Appl Catal B Environ 264:118463